On the Statistical Characterization of the Binomial Line Processes

by

Souradip Sanyal

Under the Supervision of: Dr. Gourab Ghatak

Submitted
in partial fulfillment of the requirements for the degree of
Master of Technology

to

Indraprastha Institute of Information Technology Delhi
December, 2021

Certificate

This is to certify that the thesis titled **"On the Statistical Characterization of the Binomial Line Processes"** being submitted by **Souradip Sanyal** to the Indraprastha Institute of Information Technology Delhi, for the award of the Master of Technology, is an original research work carried out by him under my supervision. In my opinion, the thesis has reached the standards fulfilling the requirements of the regulations relating to the degree.

The results contained in this thesis have not been submitted in part or full to any other university or institute for the award of any degree/diploma.

December, 2021

Dr. Gourab Ghatak
Department of Electronics and Communication Engineering
Indraprastha Institute of Information Technology Delhi
New Delhi 110 020

Acknowledgements

Throughout the entire duration of my work on this thesis I have received a great deal of support and assistance from my supervisors, peers, friends and family.

I would first like to thank my supervisor, Dr. Gourab Ghatak, whose expertise, motivation and patience was invaluable in formulating the right research question to writing this report in itself. Your timely feedback, little encouragements here and there, and overall guidance pushed me and my work to a higher level. Thank you for guiding me every step of the way.

I would also like to thank my professors, Dr.Vivek Ashok Bohara and Dr. Anubha Gupta, for their valuable guidance throughout my studies. You provided me with the tools that I needed to choose the right direction and successfully complete my thesis.

I would like to acknowledge my peers at IIITD, without whose support this thesis would have been an even more daunting challenge. In particular, I would like to sincerely thank Pallab Chakraborty, Ayush MS, Tathagat Pal and Harshal Dev for their interest, ideas and constant encouragement in my work and overall making the IIITD experience worthwhile.

Finally, I would like to thank my parents and my partner K.B. for their wise counsel and support throughout. I would sincerely love to thank you from the bottom of my heart for being with me every day and every night, especially knowing I might not have been there as much as I should have been. Thank you for believing in me when many didn't.

Abstract

This thesis introduces the Binomial Line Process (BLP) and then Binomial Line Cox Process (BLCP) based on BLP, a novel spatial stochastic model for the characterization of streets in the statistical evaluation of wireless and vehicular networks.

Stochastic Geometry based network planning is an extensively studied area. Existing models for streetwise millimeter wave network implementation include Poisson line processes (PLP), Manhattan line processes (MLP), etc. However, all of these models lack an essential aspect of city-wide street network planning: street density is denser in the city center and sparse near the suburbs. These models simulate street networks by uniformly distributing the roads on the entire $\mathbb{R}^2$ plane. Contrary to these models, the BLP model introduced here restricts the origin of the roads to a fixed circular area centered at the origin of the Euclidean plane, thereby artificially introducing inhomogeneity in street density with respect to the distance from the center. The idea being the further away we go from the city center, i.e., towards the suburbs, the sparser the entire network becomes. We have derived a closed-form expression for the contact distribution of the BLP from a random location on the plane. Leveraging this, we introduced the novel Binomial line Cox process (BLCP) to emulate points on individual lines of the BLP, where we derive the distribution of the distance of the nearest point of the Poisson line Cox process (PLCP) and the Probability Generating Functional (PGFL) of the PLCP. Based on the PGFL and the nearest point distribution, we characterize the Signal to Interference plus Noise Ratio (SINR) coverage of a network. Using these numerical results, we highlight that the network coverage characteristics from the perspective of a user at city center is remarkably different to that of a suburban user. This framework can be integrated with the existing models of line processes for a more accurate characterization of streets in urban and suburban environments.

Contents

List of Figures

List of Tables

Chapter 1

Introduction

An accurate estimation of modern cellular and vehicular communication networks need tractable models for the statistical characterization of urban infrastructure, e.g., streets, buildings, and blockages [1–3]. This is even more necessary when studying high-frequency millimeter wave (mm-wave) transmissions or vehicular networks, where network properties like access point deployment, propagation, and the location of receivers are governed by the physical objects like trees, infrastructure etc. [2, 4].
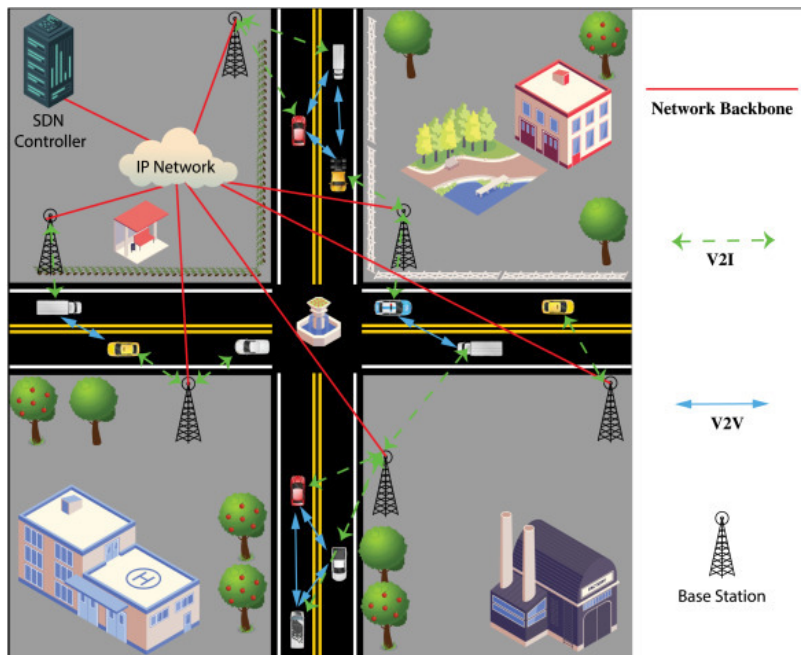
Fig. 1.1. Vehicular Communication Network: V2I stands for Vehicle to Infrastructure, while V2V is Vehicle to Vehicle Network

As we can further see from Figure 1.1, cars moving along roads with access points setup right on or beside the road whose network has to deal with infrastructure and trees needs a model where we explore the idea of access points on randomly oriented roads in cities with random blockages here and there. However, this idea can be extended to urban/suburban networks overall, where access points are located along roads, and the users may or may not be vehicular only. In this regard, stochas-
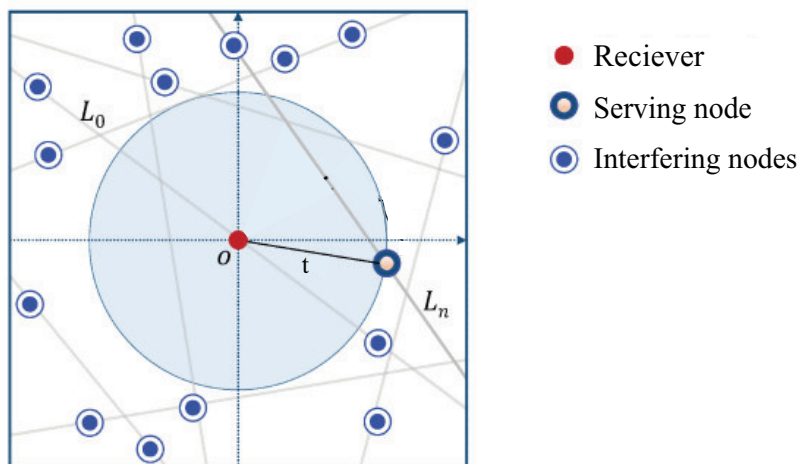
Fig. 1.2. How Access points along roads can provide network coverage to users

tic geometry based studies consider line processes for modeling streets of an urban environment [5, 6]. As we can see in Figure 1.2, the basic idea that is commonly used for line process based modelling is: Access points are located on randomly oriented streets. The user/receiver can be located anywhere along such streets or any random position (depends on the model). For the user, the nearest base station to it is considered as the serving access point, while all other base stations are considered as interference.

Out of the numerous candidate line processes, the most popular one for modeling streets in wireless communication studies is the Poisson line process (PLP) [7,8]. Here, the roads are randomly and uniformly generated throughout the plane following a Poisson Distribution, which governs the average number of roads per unit area. Although the PLP model provides significant tractability in developing performance metrics of wireless networks, it fails to accurately take into account some salient features of urban street networks such as finite street lengths and in-homogeneous density of streets across a given city. The recent work by Jeyaraj *et al.* [8] studied a generalized framework for Cox models to study vehicular networks. The authors significantly improved the accuracy of line process models to account for finite street lengths by considering t-junctions, stick processes, and Poisson lilypond models. However, their work does not consider in-homogeneous road densities e.g., dense road density in urban areas which gets increasingly sparse as we move further away from the city center. In this work, we introduce a novel line process model called the Binomial Line Process (BLP) which bridges this gap. It is envisaged that an accurate characterization of a city-wide street system will integrate the theory developed in this paper with the existing works [8].

1.1   Related Work on Line Processes

Gloaguen *et al.* [9] have modeled streets using either a Poisson-line tessellation (PLT), Poisson-Voronoi tessellation, or a Poisson-Delaunay tessellation. The PLT (the tessellation created by the PLP) has received significant interest in further re-

search, as compared to the other models due to better accuracy and applicability. For example, in the context of user equipments (UEs), the PLP model was used by Choi and Baccelli [10] to model vehicular base-stations and UEs and by Morlot [6] to model the location of UEs. The PLP was further used to study on-road deployment of mm-wave small cells in [11] and [12]. Further information in this direction can be found in [7]. To mitigate some of the drawbacks of a PLP, in particular, to take into account finite length streets, the recent work by Jeyaraj *et al.* [8] have provided a generalized framework for a class of line processes. They have considered the Poisson stick process and the lilypond model to introduce additional accurate structures like finite street length, T junctions, loops in street etc.,to the street networks. Then, using the same results, the authors have analyzed the reliability of communication networks for these different street models.

1.2 Motivation: Why One More Line Process?
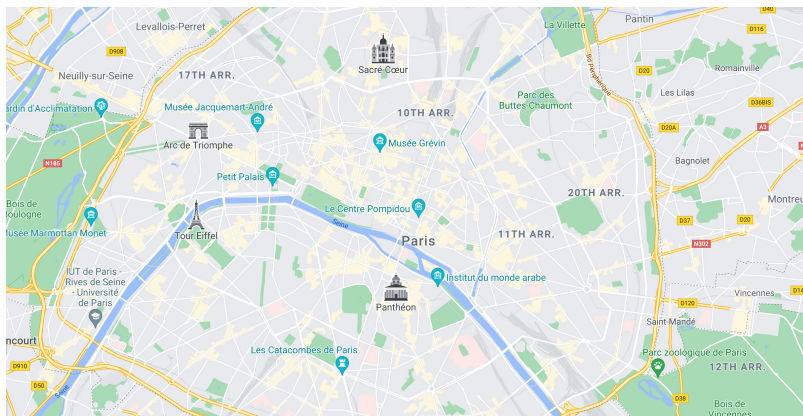
Fig. 1.3. Part of Paris city map. Visual inspection reveals the inhomogeneity of street density.

Although the literature on line processes is rich, all the above models fail to take into account a particular property of the urban infrastructure: streets are denser near the city center or downtown, while they are sparse near the suburbs. This can be observed by simple visual inspection in Fig. 1.3 where we depict a snapshot of Paris downtown and suburb. It is also important to note that in large cities, suburban connectivity is facilitated by longer streets that originate near the city centre. Such streets run through a number of residential clusters and often connect two cities.

Consider another scenario, we are inside a big industrial warehouse which stores items in bulk. The item loading and unloading is handled by an smart ASRS (Automated Storage and Retrieval System) system, involving robots/shuttles, ferrying items from one place to another along fixed paths. The warehouse is centrally organized, where every item comes in from one direction, gets sorted into different areas for storage and then gets retrieved as and when needed. The sorting and movement of items along the roads all radiating outwards from the central location of the ware-

3

house can be thought of as an instance of BLCP process, because for a big warehouse we should not expect density of roads to be uniform thoughout, just like a city.

Fig. 1.4. Warehouse with smart ASRS System

Let us elaborate this notion with the help of realizations of two candidate line processes: PLP and BLP (Please refer to Section 2.1 for details on the construction of a BLP). In Fig. 1.5, we plot a realization of a BLP (Fig. 1.5a), a PLP realization which has the same number of streets as that of the BLP (Fig. 1.5b), and a realization of a PLP which has the same street density as the BLP (Fig. 1.5c). We notice that the BLP more accurately captures the two characteristics that we intend to address: i) denser roads towards the center of the region and sparser roads towards the periphery and ii) suburbs are connected by roads that originate at the city center. Consequently, in wireless network modeling, statistical evaluation of metrics such as the distribution of the distance to the nearest street, the distance to the nearest on-street deployed access point, the number of street within a given range of a user, etc. are different for a sub-urban users and a downtown user. Thus, a study of BLP is necessary to take these nuances into account.
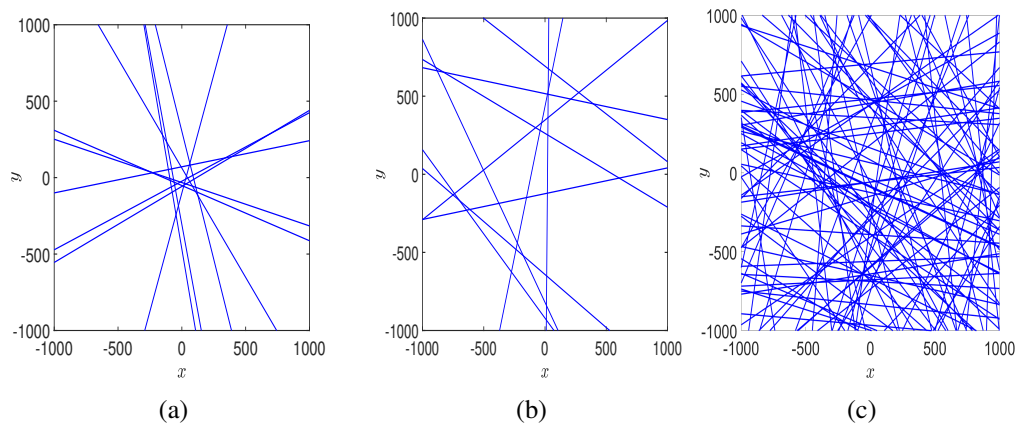

Fig. 1.5. (a) A BLP with $n_B = 10$ and $R = 100$, (b) A realization of a PLP which has 10 lines (c) A PLP with the same intensity as the BLP with $n_B = 10$.

4

1.3 Contributions

The contributions of this correspondence are as follows:

- We identified a gap in the prevailing literature, where all line process based models where considered to be homogeneous. But,in real life street densities tend to vary across urban and suburban regions.

- To plug this gap, we introduce and characterize the BLP, which is a novel spatial stochastic model to characterize streets jointly in an urban and suburban environment. To the best of our knowledge, the BLP has never been studied in wireless network modeling.

- We introduce the notion of *domain bands*, which are subsets of the generating set of the BLP that correspond to lines which intersect a given disk in $\mathbb{R}^2$. We derive exact expression for the area of the domain bands. Consequently, we derive the void probability of the domain bands in the generating domain, which correspond to the probability that no lines intersect a given given disk in $\mathbb{R}^2$. We extend this framework to derive the distance distribution of the nearest line from an arbitrary point on the Euclidean plane.

- Leveraging the above, we introduce a doubly stochastic process called the BLCP which models locations on individual streets as a 1D Poisson point process (PPP). We derive the distance distribution of the nearest BLCP point from a given location in $\mathbb{R}^2$.

- Based on the above introduction to BLP and BLCP, we have derived the PGFL of the BLCP. This in turn, enabled us to do a SINR analysis of this setup.

- Finally, we have compared the results obtained with this framework with the traditional PLP and PLCP setup to highlight the differences.

It must be noted that the objective of this thesis is not to propose a model that completely replaces existing stochastic geometry models for characterizing streets and on-street locations in a wireless network, e.g., PLP and PLCP, respectively. On the contrary, the proposed framework can be integrated into the existing models to increase their accuracy, by jointly taking into account the relative inhomogeneity of street and therefore network configurations for an urban and sub-urban user.

Chapter 2

Binomial Line Process

A line process $\mathcal{P} \subset \mathbb{R}^2$ is a collection of lines $\{L_1, L_2, \ldots\}$ in $\mathbb{R}^2$. In this chapter, we shall introduce the BLP and derive various results from the same to gain insight on how it differs from the standard PLP, that has been used for modelling so far.

2.1 Construction

Let us denote a BLP by $\mathcal{P}_B$, which is a collection of a fixed n_B number of lines. Any line that belongs to $\mathcal{P}_B$ is uniquely characterized by the distance r_i between the origin O and its projection P on the line, and by the angle θ between $\vec{OP}$ and the x-axis on the other hand. For a BLP, the domain of the pair of parameters (θ, r_i) is the finite cylinder $\mathcal{D} := [0, 2\pi] \times [0, R]$. We will call $\mathcal{D}$ as the generating set or the domain set of $\mathcal{P}_B$, and a point $(\theta_i, r_i) \in \mathcal{D}$, corresponding to a line $L_i \in \mathcal{P}_B$, the generating point of L_i. Accordingly, there is a bijective mapping $f : \mathcal{P}_B \to \mathcal{D}$ between any random point $(\theta_i, r_i) \in \mathcal{D}$ and a corresponding line $L_i \in \mathcal{P}_B$. We can now define a BLP, formally.

Definition 1. *A line process $\mathcal{P}_B \triangleq \{L_i\}$ in $\mathbb{R}^2$ consisting of n_B lines is a BLP, if and only if the set of corresponding n_B generating points $\{(\theta_i, r_i) = f(L_i)\}$ is a Binomial Point Process (BPP) in $\mathcal{D}$.*
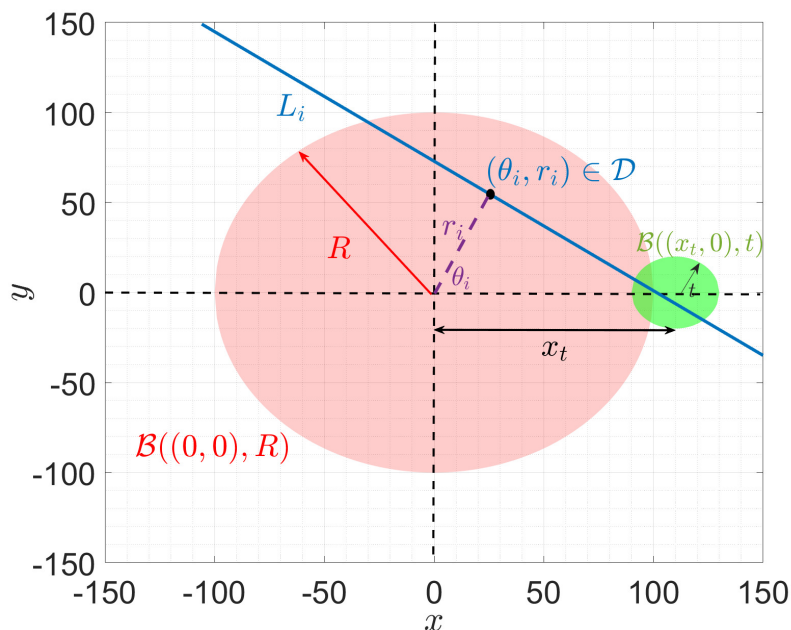
Fig. 2.1. Illustration of the construction of a BLP and intersecting lines on $\mathcal{B}((x_t, 0), t)$.

This is elaborated further in Fig. 2.1, which is an example of BLP with 1 line and where the generating points of the lines are restricted to the disk $\mathcal{B}((0,0), R)$ (a disc of radius $\mathcal{R}$, centered at (0,0)). The crucial point to note is: The number of points (and thus lines corresponding to those points) are fixed and they are randomly and uniformly oriented within the disc $\mathcal{B}((0,0), R)$ .Furthermore, we note that unlike stationary point processes, the statistics of the BLP cannot be studied from the perspective of a typical point due the inherent heterogeneity outside and inside the disk. However, due to the isotropic construction of the BLP (since the points inside the circle are located at random), we can assume that the "average" properties of the BLP as seen from a point depends only on its distance from the center and not its orientation (Each instance of the process might have varying values, so we are taking about averages here). Accordingly, without loss of generality, let us consider a test point located at $(x_t, 0)$. First, we study the set of lines that intersect a randomly located disk of radius t in $\mathbb{R}^2$ centered around a test point $(x_t, 0)$ (as shown by the green circle in the Figure 2.1). We shall use this setup to calculate the CDF of the distance to the nearest BLP line for a random point in the upcoming sections (specifically Section 2.4).

2.2 Domain bands in $\mathcal{D}$

The equation of the line L_i corresponding to $(\theta_i, r_i) \in \mathcal{D}$ is given by:
$x \cos(\theta_i) + y \sin(\theta_i) = r_i.$

On the other hand, the equation of the circle $\mathcal{B}_p((x_t, 0), t)$ with the test node at its center and a radius of t is given by: $(x - x_t)^2 + y^2 = t^2$.

Now, for any straight line given by the equation: $ax + by + c = 0$, the perpendicular distance of the line from the point $(x_t, 0)$ is given by:

$$\frac{|ax_t + c|}{\sqrt{a^2 + b^2}}.$$

So, in our case, distance of the line L_i from $(x_t, 0)$ is:

$$d_{Li} = |x_t \cos(\theta_i) - r_i| \tag{2.1}$$

In order to find the set of (θ_i, r_i) for which L_i intersects $\mathcal{B}((x_t, 0), t)$, we need to find the (θ_i, r_i) which results in $d_{Li} \leq t$. So, we get that, L_i intersects $\mathcal{B}((x_t, 0), t)$ for:

$$x_t \cos(\theta_i) - t \leq r_i \leq x_t \cos(\theta_i) + t. \tag{2.2}$$
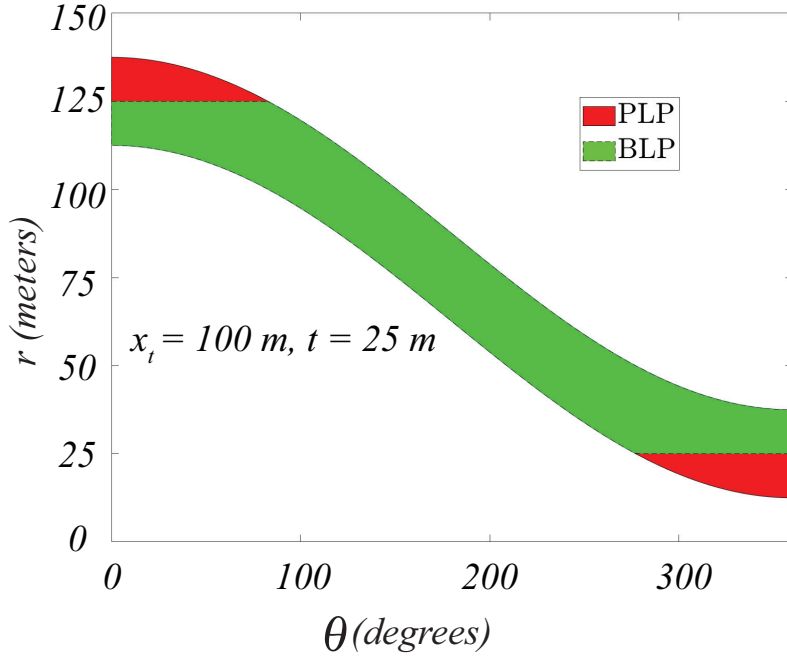
Fig. 2.2. Set of points in $\mathcal{D}$ which generate lines in $\mathbb{R}^2$ that intersect $\mathcal{B}((x_t, 0), t)$ for a BLP (denoted by green) and a PLP (denoted by red). Note that the part of the red region behind the green region is hidden. Here $R = 100$.

In Fig. 2.2, we show the set of points in $\mathcal{D}$ that generate lines in $\mathbb{R}^2$ intersecting $\mathcal{B}_p((x_t, 0), t)$. Due to their structure, henceforth they are referred to as *domain bands*. It is interesting to note that the domain band for the BLP is a clipped version of the PLP due to the restriction of the points to lie within $\mathcal{B}((0, 0), R)$.
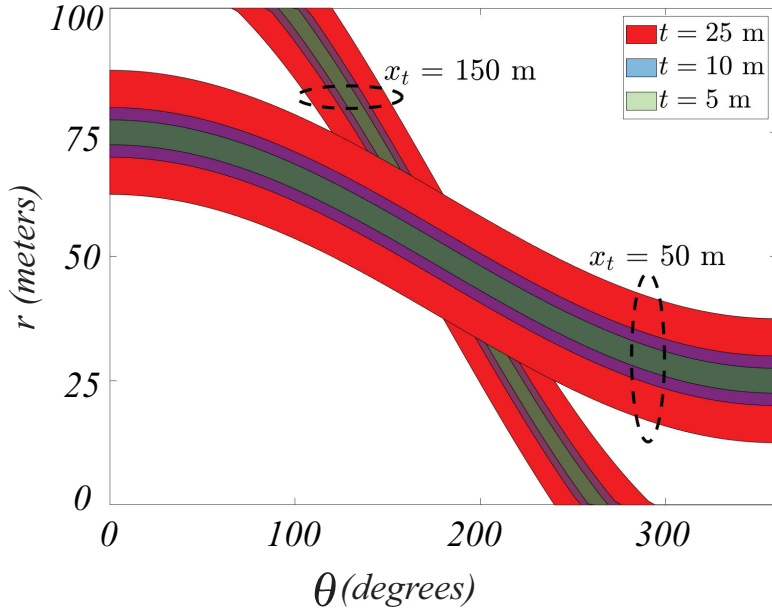
Fig. 2.3. Domain bands for different values of t and x_t. Here $R = 100$. Note that when $|x_t| + t \leq R$, the domain bands for PLP and BLP coincide.

In Fig. 2.3, we plot the domain bands for the BLP for different values of x_t and t. We note that when $|x_t| + t < R$, the domain bands for BLP and PLP coincide. Additionally, the width of the band decreases as t decreases or x_t increases. As we will see in the next section.

2.3   Void Probabilities

Corollary 1. *The area of the domain band for a PLP is independent of x_t.*

This can be easily verified by evaluating the following:

$$\int_0^\pi (x_t \cos(\theta) + t)\, \mathrm{d}\theta - \int_0^\pi (x_t \cos(\theta) - t)\, \mathrm{d}\theta = 2\pi t.$$

The classical result of PLP follows from above.

Corollary 2. *The number of lines intersecting $\mathcal{B}((0, x_t), t)$ is Poisson distributed with parameter $2\pi t$. Accordingly, the probability that no lines intersect $\mathcal{B}((0, x_t), t)$ is given by $\exp(-2\pi \lambda x_t)$.*

For a BLP, however, the area of the domain band needs to be calculated explicitly. For the same, let us first note that the values of θ_i for which r_i, as given by (2.2), exceeds $\pm R$ is:

$$\theta_{11}(x_t, t) = \cos^{-1}\left(\frac{R - t}{x_t}\right), \quad \theta_{12}(x_t, t) = \cos^{-1}\left(\frac{R + t}{x_t}\right),$$

9
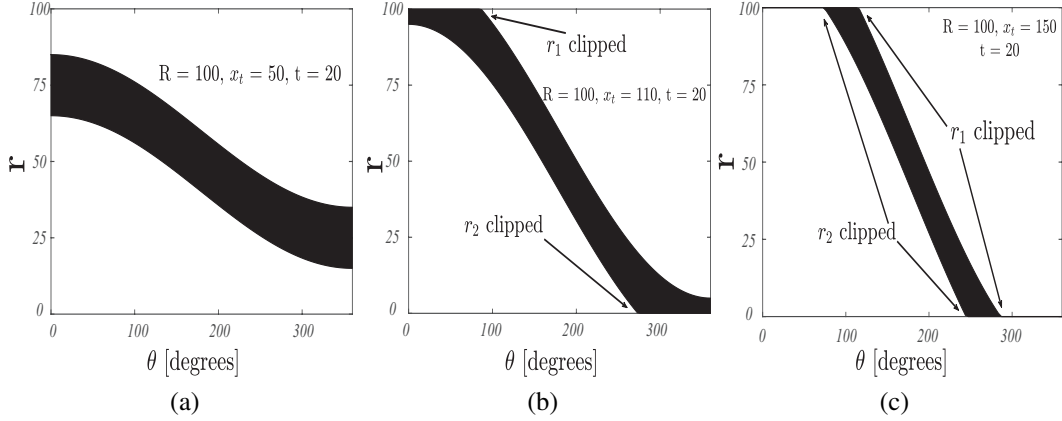
Fig. 2.4. (a) Case 1: $|x_t| + t \leq R$ (b) Case 2 $|x_t| + t \geq R$ and $|x_t| - t \leq R$ and (c) Case 3: $|x_t| - t \geq R$.

$$\theta_{21}(x_t, t) = \cos^{-1}\left(-\frac{R-t}{x_t}\right) = \pi - \theta_{11}(x_t, t),$$

$$\theta_{22}(x_t, t) = \cos^{-1}\left(-\frac{R+t}{x_t}\right) = \pi - \theta_{12}(x_t, t). \tag{2.3}$$

We have now developed the necessary tools to evaluate the area of the domain band for a BLP, which is presented below.

Theorem 1. *The area of the domain band for a BLP $\mathcal{P}_B$ defined on $[0, \pi) \times [-R, R]$ corresponding to $\mathcal{B}(x_t, t)$ is:*

$$\mathcal{A}_D(x_t, t) = \begin{cases} 2\pi t; & \text{for } |x_t| + t \leq R \\ 2\left[\pi t - x_t\sqrt{1 - \left(\frac{R-t}{x_t}\right)^2} + (R-t)\cos^{-1}\left(\frac{R-t}{x_t}\right)\right]; \\ \qquad \text{for } |x_t| + t > R \text{ and } |x_t| - t \leq R \\ 2\left[\pi t - x_t\left(\sqrt{1 - \left(\frac{R-t}{x_t}\right)^2} - \sqrt{1 - \left(\frac{R+t}{x_t}\right)^2}\right)\right. \\ \left. + (R-t)\cos^{-1}\left(\frac{R-t}{x_t}\right) - (R+t)\cos^{-1}\left(\frac{R+t}{x_t}\right)\right]; \\ \qquad \text{for } |x_t| - t \geq R \end{cases} \tag{2.4}$$

Proof. Let us consider three cases below:

Case 1: $|x_t| + t \leq R$**.** (Refer to Fig. 2.4a). Here, naturally we have $|x_t| - t \leq R$. For this case, the domain band for the BLP coincides with that of the PLP. Accordingly, the area of the domain band for Case 1 is $\mathcal{A}_{D1}(x_t, t) = 2\pi t$.

Case 2: $|x_t| + t > R$ and $|x_t| - t \leq R$.(Refer to Fig. 2.4b). In this case, the upper part of the band is clipped on the left, and the lower part of the band is clipped

on the right. Noting the symmetry of the domain bands from the perspective of the $\theta = \frac{\pi}{2}$ line, the area is evaluated as:

$$\mathcal{A}_{D2}(x_t, t) = 2\left(\pi t - ClippedArea\right)$$

$$= 2\pi t - 2\int_0^{\cos^{-1}\left(\frac{R-t}{x_t}\right)} \left(x_t \cos(\theta) + t\right) \mathrm{d}\theta$$

$$+ 2\int_0^{\cos^{-1}\left(\frac{R-t}{x_t}\right)} R\,\mathrm{d}\theta$$

Case 3: $|x_t| - t > R$**.** (Refer to Fig. 2.4c). Here, naturally, $|x_t| + t > R$. In this case, both the lower and the upper part of the domain band is clipped on both left and right ends, so in a similar manner to the above case, the area of the domain band is:

$$A_{D3}(x_t, t) = 2\left(\pi t - ClippedArea\right)$$

$$= 2\pi t - 2\int_0^{\cos^{-1}\left(\frac{R+t}{x_t}\right)} \left[(x_t \cos(\theta) + t) - (x_t \cos(\theta) - t)\right] \mathrm{d}\theta$$

$$- 2\int_{\cos^{-1}\left(\frac{R+t}{x_t}\right)}^{\cos^{-1}\left(\frac{R-t}{x_t}\right)} \left(x_t \cos(\theta) + t\right) \mathrm{d}\theta + 2\int_{\cos^{-1}\left(\frac{R+t}{x_t}\right)}^{\cos^{-1}\left(\frac{R-t}{x_t}\right)} R\,\mathrm{d}\theta$$

Evaluating the above integrals for Case 2 and Case 3 completes the proof. $\qquad\square$

This expression, however is only one of possible ways of representing the *Domain Band*. As seen here, the expression for A_d depends on x_t, t and R. But, as we shall see ahead, a more convenient way of expressing this Domain Band, is in terms of (r, θ) pair, such that $(r, \theta) \in \mathcal{D}$ and $\iint_D dr d\theta = A_d$. For deriving such an expression, we refer to equation (2.2), while keeping in mind that: $-R \leq r_i \leq R$, as $r_i \in B((0,0), R)$ (as described in Section 2.1). This is the expression we get, which clearly maintains the dependency on x_t, t and R :

We begin by defining $\theta_1 \ \ and \ \ \theta_2$ as follows:

$$\theta_1 = \begin{cases} \cos^{-1}\left(\frac{R+t}{x_t}\right) & if \quad x_t > R + t \\ 0 & otherwise \end{cases}$$

$$\theta_2 = \begin{cases} \cos^{-1}\left(\frac{R-t}{x_t}\right) & if \quad x_t > R - t \\ 0 & otherwise \end{cases}$$

Leveraging these 2 values of θ, we can divide the region $\mathcal{D}$ into 3 smaller regions, each with its own set of limits on (r, θ). These equations are summarized below:

r	θ
$x_t cos\theta - t \to R$	$\theta_1 \to \theta_2$
$-R \to x_t cos\theta + t$	$\pi - \theta_2 \to \pi - \theta_1$
$x_t cos\theta - t \to x_t cos\theta + t$	$\theta_2 \to \pi - \theta_2$

Table 2.1: (r, θ) limits for valid points which fall in $\mathcal{D}$

Please note that: A valid representation of the *Domain Band* involves a sum of 3 integrations over the (r, θ) domain, as described in Table 2.1. Going forward, we shall leverage the fact: $(r, \theta) \in \mathcal{D} \implies (r, \theta)$ must be in the limits as described by Table 2.1 to write:

$$\int_{\theta_1}^{\theta_2} \int_{x_t cos\theta - t}^{R} f(r, \theta) \quad dr d\theta + \int_{\pi - \theta_2}^{\pi - \theta_1} \int_{-R}^{x_t cos\theta + t} f(r, \theta) \quad dr d\theta$$

$$+ \int_{\theta_2}^{\pi - \theta_2} \int_{x_t cos\theta - t}^{x_t cos\theta + t} f(r, \theta) \quad dr d\theta = \iint_{A_d} f(r, \theta) \quad dr d\theta$$

Corollary 3. *The probability that no line of the BLP intersects with $\mathcal{B}((x_t, 0), t)$ is given by:*

$$\mathcal{V}_B \left(\mathcal{B}((x_t, 0), t) \right) = \left(\frac{2\pi R - \mathcal{A}_{\mathcal{D}}(x_t, t)}{2\pi R} \right)^{n_B} \tag{2.5}$$

In other words, $P($No BLP line is within distance t of $(x_t, 0) = \mathcal{V}_B$. Consequently, the cumulative density function (CDF) of the distance to the nearest line from $(x_t, 0)$ is given in the following lemma.

2.4 Nearest Line Distribution

Lemma 1. *For the point $(x_t, 0)$, the CDF of the distance to the nearest line of the BLP is given by:*

$$F_d(t) = 1 - \mathcal{V}_B \left(\mathcal{B}((x_t, 0), t) \right) \tag{2.6}$$
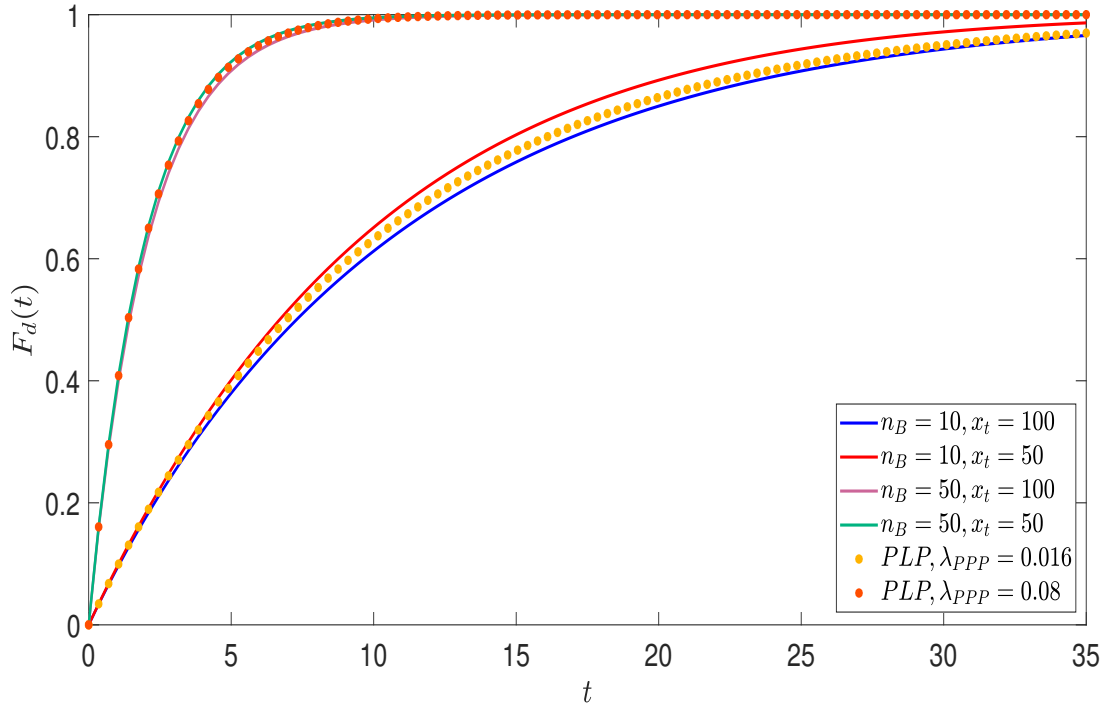
Fig. 2.5. Distance distribution of the nearest line from $(x_t, 0)$.

In Fig. 2.5 we plot the CDF for different values of n_B and x_t. For comparison, we have also included the CDF of the nearest line of a PLP with the same intensity λ^{PPP} as that of a BLP ($\frac{n_B}{2\pi R}$) with $n_B = 10$ and $n_B = 50$ points for $R = 100$. Noticeably the nearest line is statistically closer for a larger value of n_B and lower value of x_t. This inference is missed by the CDF of the distance to the nearest line in a PLP, where the CDFs coincide for all values of x_t for a given λ^{PPP}. Thus, we note how a BLP process differs from a standard PLP Process. Next, we shall analyze how network access points based on streets governed by such a BLP process behaves.

Chapter 3

Binomial Line Cox Processes

For each line $L_i \in \mathcal{P}_B$, let us define a 1D PPP Φ_i with intensity λ. We assume that Φ_i is independent of Φ_j for $L_i \neq L_j$. The set of all such points created is defined as a BLCP. The ID PPP represents, the network access points located Independently and Identically on the roads generated by the BLP Process. Next, we derive the distance distribution to the nearest BLCP point from $(x_t, 0)$. The objective being to calculate where the nearest access point is located for a random user at $(x_t, 0)$.

3.1 Distance Distributions

We begin again with figure 2.1, where we showed the construction for a BLP and expand on it.

Fig. 2.1. BLP and its construction
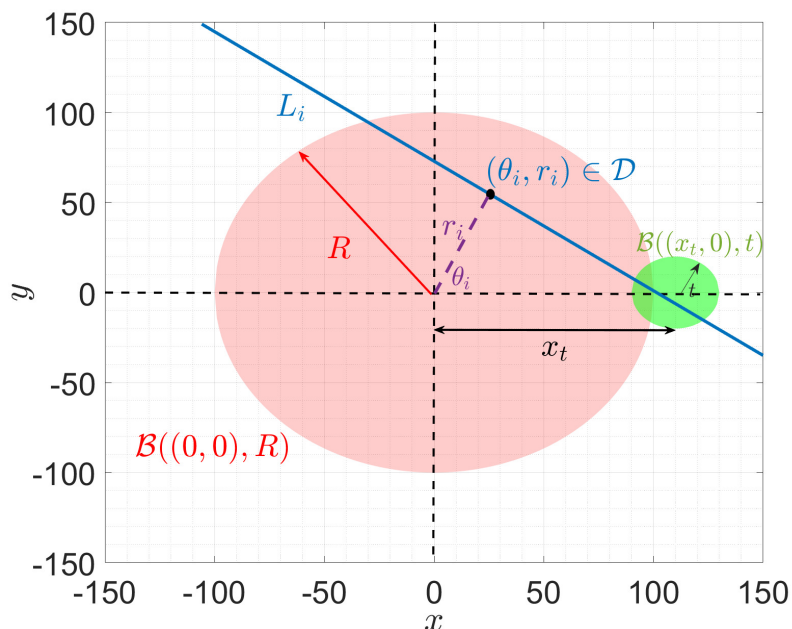
For the BLCP, points are distributed according to a PPP on lines such as L_i, and we assume that there are n_B such lines in the original BLP.

First, we compute the void probability of a given line L_i characterized by its (r, θ) value.

Theorem 2. *The probability that no BLCP point will fall inside $B((x_t, 0), t)$ given that there is one BLP line at (r, θ) and the PPP for the BLCP Process has intensity λ is:*

$$v_{BLCP} = \frac{1}{2\pi R} \int_0^R \int_0^{2\pi} e^{-\lambda C(r,\theta)} \, d\theta \, dr \tag{3.1}$$

$$where, C(r, \theta) = \begin{cases} 2\sqrt{t^2 - (x_t cos\theta - r)^2} & when, \quad t \geq |x_t cos\theta - r| \\ 0 & otherwise \end{cases} \tag{3.2}$$

Proof. As we saw in Equation 2.1 in Chapter 2.2, the distance of the line L_i from $(x_t, 0)$ point is: $|x_t cos\theta - r|$. So, length of a chord passing through $B((x_t, 0), t)$ is:

$$C_{Length} = 2\sqrt{t^2 - (x_t cos\theta - r)^2}, \quad t \geq |x_t cos\theta - r| \tag{3.3}$$

Now, given that a line characterized by (r, θ) passes through $\mathcal{B}((x_t, 0), t)$, the probability that no points of the PPP will fall on that chord is given by: $exp(-\lambda C_{Length})$.

Now, overall with $n_B = 1$, and a region R given by $\mathcal{B}((x_t, 0), t)$:

$P(\text{No points of PLCP fall within } R) = P(\text{The PLP line does not intersect with } R) + P(\text{The PLP line falls within } R \text{ but there are no PLCP points on the chord})$

$$\implies v_{BLCP} = \left(1 - \frac{A_d}{2\pi R}\right) + \left(\frac{A_d}{2\pi R}\right)\left(\frac{1}{A_d}\right) \iint\limits_{A_d} e^{-\lambda C_{Length}} \, dr \, d\theta$$

$$= \left(\frac{1}{2\pi R}\right) \iint\limits_{2\pi R - A_d} dr \, d\theta + \left(\frac{1}{2\pi R}\right) \iint\limits_{A_d} e^{-\lambda C_{Length}} \, dr \, d\theta$$

$$= \left(\frac{1}{2\pi R}\right) \left[\iint\limits_{2\pi R - A_d} e^0 \, dr \, d\theta + \iint\limits_{A_d} e^{-\lambda C_{Length}} \, dr \, d\theta \right]$$

$$= \left(\frac{1}{2\pi R}\right) \iint\limits_{2\pi R} e^{-\lambda C(r,\theta)} \, dr \, d\theta$$

$$= \frac{1}{2\pi R} \int_0^R \int_0^{2\pi} e^{-\lambda C(r,\theta)} \, d\theta \, dr$$

Where, C_{Length} is as described in equation 3.3 and C(r, θ) is as described by equation 3.2. Note that: $C = C_{Length} = 0$, when $(r, \theta) \notin \mathcal{D}$ or, $(r, \theta) \in (2\pi R - A_d)$.

□
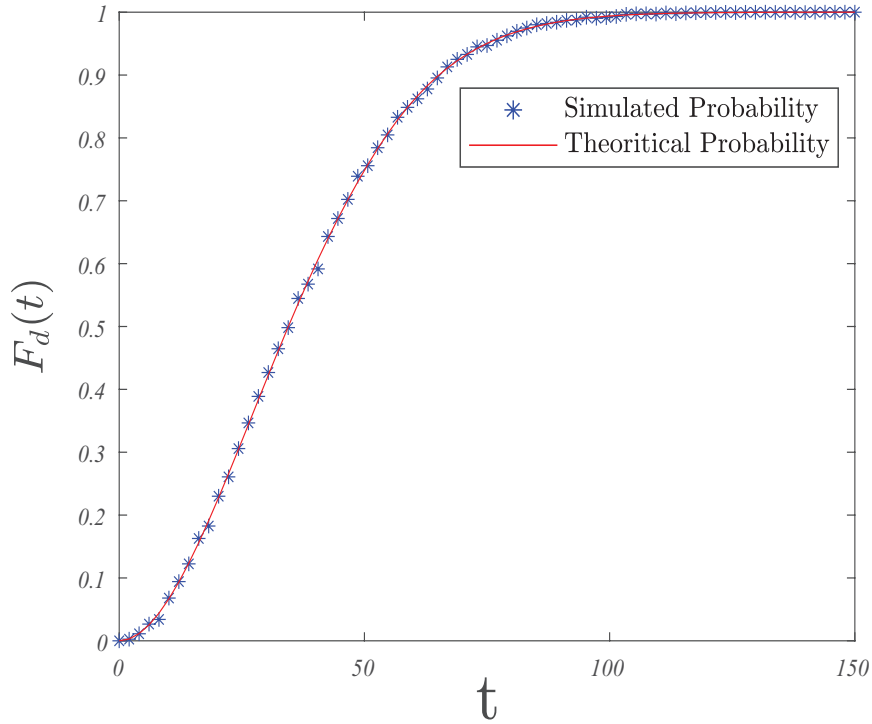
Fig. 3.1. Distance distribution of the nearest BLCP from $(x_t, 0)$. $x_t = 150$, R = 100 and $n_B = 10$ for this setup.

With the void probability of a BLCP line calculated, we are now equipped to calculate the nearest point distribution for BLCP process.

Corollary 4. *The distribution of the nearest BLCP point to the point $(x_t, 0)$ for n_B BLP points, is given by:*

$$F_D(t) = 1 - \left(\frac{1}{2\pi R} \int_0^R \int_0^{2\pi} e^{-\lambda C(r,\theta)} \, d\theta \, dr \right)^{n_B} \tag{3.4}$$

Proof.

$$
\begin{aligned}
F_D(t) &= P[\text{Min(Distance)} \leq t] \\
&= 1 - P[\text{Min(Distance)} > t] \\
&= 1 - P[\text{Distance of all BLCP Points} > t] \\
&= 1 - (P[\text{No BLCP Points fall within t}])^{n_B} \\
&= 1 - (v_{BLCP})^{n_B}
\end{aligned}
$$

$\square$

16

3.2 Probability Generating Functional

Apart from the distance distributions, another useful metric for Line Processes is Probability Generating Functional (PGFL).

We define PGFL for a function f(x_i) over any Line Process Φ as:

$$G = \mathop{\mathbb{E}}_{\Phi} \left(\prod_{i=1}^{n} f(x_i) \right), \text{ for n total points in the Line Process } \Phi.$$

Theorem 3. *For a BLP with n_B lines, the PGFL of a function $f(x_i)$ is given by:*

$$G(x_t, R, n_B) = \left[\frac{\int_0^{2\pi} \int_0^R exp\left(-2\lambda \int_0^{\infty} 1 - f\left(\sqrt{y^2 + (x_t cos\theta - r)^2} \right) dy \right) dr \, d\theta}{2\pi R} \right]^{n_B}$$

$$(3.5)$$

Proof. We begin with the PGFL expression for a PPP process. We can then take an expectation of that value over the lines in the BLP process. In the book "Poisson Line Cox Process: Foundations and Applications to Vehicular Networks Synthesis Lectures", Harpreet *et al.* [13], showed that for a PPP (Poisson Point Process) of intensity λ and a function f is (for d dimensional plane for the PPP):

$$G = exp(-\lambda \int_{\mathbb{R}^d} (1 - f(x))dx)$$

We shall derive here the PGFL expression for a BLCP process. First, we note the following things from Figure 3.2:
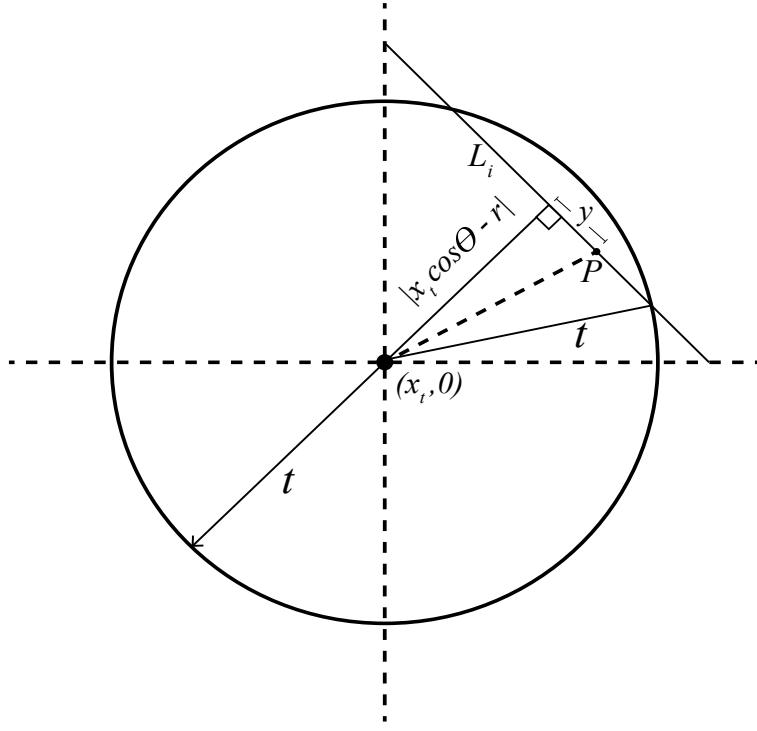
Fig. 3.2. Setup for Calculating PGFL of BLCP.

- Distance of the BLP Line L_i from the point $(x_t, 0) = |x_t \cos \theta - r|$.

- We are taking a random point P, located at a distance 'y' from the midpoint of chord.

- The distance of the point P from the center point or $(x_t, 0)$ is:
  $\sqrt{y^2 + (x_t \cos \theta - r)^2}$

- The length of the chord, as given by Equation 3.3 is: $2\sqrt{t^2 - (x_t \cos \theta - r)^2}$, however it is easier to work with half of this chord length and in turn double the PLP intensity 2λ. So, we define the length of the chord from its midpoint to the point where it touches the circle as:

$$C(t) = \begin{cases} \sqrt{(t^2 - (x_t \cos \theta - r)^2)}, & t \geq |x_t \cos \theta - r| \\ 0, & otherwise \end{cases} \tag{3.6}$$

Thus, for a single BLP line L_i, characterized by $(r, \theta) \in \mathcal{D}$ and $C(t)$ as described in Equation 3.6 :

$$G_t''(t, x_t, r, \theta) = exp\left(-2\lambda \int\limits_0^{C(t)} 1 - f\left(\sqrt{y^2 + (x_t cos\theta - r)^2}\right) dy\right) \tag{3.7}$$

18

Now, averaging over $\forall (r, \theta) \in \mathcal{D}$, with $G_t''(t, x_t, r, \theta)$ from Equation 3.7:

$$G_t'(t, x_t, R) = \left(\frac{\iint\limits_{A_d} G_t''(t, x_t, r, \theta) \, dr \, d\theta}{A_d} \right) \tag{3.8}$$

Leveraging this result, we shall now average this PGFL expression across all n_B lines in the BLP by calculating $\underset{\Phi_{BLP}}{\mathbb{E}} \, G_t'(t, x_t, R)$, with $G_t'(t, x_t, R)$ as calculated in Equation 3.8:

$$G_t(t, x_t, R, n_B) = \underset{\Phi_{BLP}}{\mathbb{E}} \, G_t'(t, x_t, R)$$

$$G_t'(t, x_t, R) = \sum_{n=0}^{n_B} \binom{n_B}{n} \left(\frac{A_d}{2\pi R} \right)^n \left(1 - \frac{A_d}{2\pi R} \right)^{n_B - n} (G_t'(t, x_t, R))^n$$

$$= \sum_{n=0}^{n_B} \binom{n_B}{n} \left(\frac{A_d}{2\pi R} \right)^n \left(\frac{2\pi R - A_d}{2\pi R} \right)^{n_B - n} \left(\frac{1}{A_d} \iint\limits_{A_d} G_t''(t, x_t, r, \theta) \, dr \, d\theta \right)^n$$

$$= \left(\frac{1}{2\pi R} \right)^{n_B} \sum_{n=0}^{n_B} \binom{n_B}{n} (2\pi R - A_d)^{n_B - n} \left[\iint\limits_{A_d} G_t''(t, x_t, r, \theta) \, dr \, d\theta \right]^n$$

$$= \left(\frac{1}{2\pi R} \right)^{n_B} \left(\iint\limits_{A_d} G_t''(t, x_t, r, \theta) \, dr \, d\theta + 2\pi R - A_d \right)^{n_B}$$

$$= \left(\frac{1}{2\pi R} \right)^{n_B} \left[\iint\limits_{A_d} exp\left(-2\lambda \int\limits_0^{C(t)} 1 - f\left(\sqrt{y^2 + (x_t cos\theta - r)^2} \right) dy \right) dr \, d\theta \right.$$

$$\left. + \iint\limits_{2\pi r - A_d} exp(-2\lambda \, 0) \, dr \, d\theta \right]^{n_B}$$

$$= \left(\frac{1}{2\pi R} \right)^{n_B} \left[\int\limits_0^R \int\limits_0^{2\pi} exp\left(-2\lambda \int\limits_0^{C(t)} 1 - f\left(\sqrt{y^2 + (x_t cos\theta - r)^2} \right) dy \right) dr \, d\theta \right]^{n_B}$$

19

Thus, we are getting:

$$G_t(t, x_t, R, n_B) = \left[\frac{\int_0^{2\pi} \int_0^R exp\left(-2\lambda \int_0^{C(t)} 1 - f\left(\sqrt{y^2 + (x_t cos\theta - r)^2}\right) dy\right) dr\, d\theta}{2\pi R} \right]^{n_B}$$

(3.9)

Now, as we can notice in Equation 3.6, in the expression for $G_t(t, x_t, R, n_B)$, only $C(t)$ depends on t. For actual PGFL, we need consider values from all points, so:

$$G(x_t, R, n_B) = \lim_{t \to \infty} G_t(t, x_t, R, n_B)$$

(3.10)

Now, from Equations 3.10 and 3.6, we get:

$$\lim_{t \to \infty} G_t(t, x_t, R, n_B) = G(x_t, R, n_B) \text{ and } \lim_{t \to \infty} C(t) = \infty$$

Finally, using the above 2 equations, we get:

$$G(x_t, R, n_B) = \left[\frac{\int_0^{2\pi} \int_0^R exp\left(-2\lambda \int_0^\infty 1 - f\left(\sqrt{y^2 + (x_t cos\theta - r)^2}\right) dy\right) dr\, d\theta}{2\pi R} \right]^{n_B}$$

This completes our proof for the PGFL of BLCP Process.

□

In the next section, we shall do the SINR Coverage analysis for a network modelled by such a BLCP Process using all of the results derived so far in this chapter.

Chapter 4

SINR Coverage Analysis

In this chapter, we shall finally see a network approximated by a BLCP model and see how the SINR coverage analysis of such a model holds up to the more traditional PLCP model. This will in-turn give us some empirical estimate of how much the constraints of this newly introduced model impact the coverage probability estimate for a typical user.

4.1 Setup for the BLCP Model

Before we begin with characterization of the network, we shall introduce the Setup we used/the parameters we assumed for this model

- We are assuming a Typical User model, where a network user is randomly placed in the network at any point, and we shall derive the characteristics of the network based on the signal received by that random user.

- We assume a RSSI(Received Signal Strength Indicator) based association of the typical user. Here, the typical user is connected to the antenna which is the nearest to that user, and thus presumably has higher transmit power compared to all other antennas nearby. So, that automatically means that all other antennas excepting the nearest antenna are automatically considered as interferers for this system.

- We have a single tier network, all operating on the same carrier frequency. On top of that, the channel is a Rayleigh Fading Channel with unit power, such that:

$$R_X \text{ Power} = h_i P d_i^{-\alpha}$$

where, P is the transmitted signal power, d_i is the distance between the transmitter and the receiver, h_i is the channel fading, with $h_i \sim exp(1)$ (Exponential Density with $\mu = 1$), and finally, $\alpha \geq 2$ is the path loss coefficient for the channel.

4.2   SINR Coverage Probability for typical networks

For a typical network, we define SINR (Signal to Interference plus Noise Ratio) coverage probability as:

$$P_{coverage} = P[SINR > \gamma]$$

$$\text{With, } SINR = \frac{KPd_1^{-\alpha}h_1}{N_0 + \sum\limits_{\Phi/\{x_1\}} KPd_i^{-\alpha}h_i} \tag{4.1}$$

Here, $\sum\limits_{\Phi/\{d_1\}} KPd_i^{-\alpha}h_i$ is the interference term. $\Phi/\{d_1\}$ represents all the interferers, that is, the BLCP process Φ minus the nearest base station which is associated with the user. We consider the nearest base station x_1 is located at a distance d_1 from the user. Lastly, N_0 is the noise power, h_i is the fading for each channel, which is assumed to be i.i.d. and K is a constant factor.

Theorem 4. *For any single tier network, the SINR coverage probability for the described scenario is given by:*

$$P_{Coverage} = \underset{d_1}{\mathbb{E}} \left[\exp\left(\frac{-\gamma N_0}{KPd_1^{-\alpha}}\right) G_{\Phi'}\left(\frac{1}{1 + \frac{\gamma d_i^{-\alpha}}{d_1^{-\alpha}}}\right) \right] \tag{4.2}$$

Where, $G_{\Phi'}$ is the PGFL over $\Phi' = \Phi/\{x_1\}$.

Proof.

$$P_{Coverage} = P\left[\frac{KPd_1^{-\alpha}h_1}{N_0 + \sum\limits_{\Phi'} KPd_i^{-\alpha}h_i} > \gamma \right]$$

$$= P\left[h_1 > \frac{\gamma \sum\limits_{\Phi'} KPd_i^{-\alpha}h_i + \gamma N_0}{KPd_1^{-\alpha}} \right]$$

$$= \underset{d_1,\Phi,h_i}{\mathbb{E}}\left[\frac{\gamma \sum\limits_{\Phi'} KPd_i^{-\alpha}h_i + \gamma N_0}{KPd_1^{-\alpha}} \right]$$

[Using the CCDF of Exponential Distribution]

$$= \mathbb{E}_{d_1} \left[\exp\left(\frac{-\gamma N_0}{KPd_1^{-\alpha}} \right) \mathbb{E}_{\Phi',h_i} \left[\exp\left(\frac{-\gamma \sum_{\Phi'} h_i}{d_i^{-\alpha}} \right) \right] \right]$$

Here, the 1st term: $\exp\left(\frac{-\gamma N_0}{KPd_1^{-\alpha}} \right)$, is due to noise and thus only depends on d_1 and N_0.

The second term: $\mathbb{E}_{\Phi',h_i} \left[\exp\left(\frac{-\gamma \sum_{\Phi'} h_i}{d_i^{-\alpha}} \right) \right]$, is due to interference and can be further simplified as:

$$\mathbb{E}_{\Phi',h_i} \left[\exp\left(\frac{-\gamma \sum_{\Phi'} h_i}{d_i^{-\alpha}} \right) \right] = \mathbb{E}_{\Phi'} \left[\mathbb{E}_{h_1} \left[\prod_{\Phi'} \exp\left(\frac{-\gamma d_i^{-\alpha} h_i}{d_1^{-\alpha}} \right) \right] \right]$$

$$= \mathbb{E}_{\Phi'} \left[\prod_{\Phi'} \left[\mathbb{E}_{h_1} \exp\left(\frac{-\gamma d_i^{-\alpha} h_i}{d_1^{-\alpha}} \right) \right] \right]$$

$$= \mathbb{E}_{\Phi'} \left[\prod_{\Phi'} \left[\mathbb{E}_{h_1} \exp\left(\frac{-\gamma d_i^{-\alpha}}{d_1^{-\alpha}} h_i \right) \right] \right]$$

$$= \mathbb{E}_{\Phi'} \left[\prod_{\Phi'} \frac{1}{1 + \frac{\gamma d_i^{-\alpha}}{d_1^{-\alpha}}} \right]$$

[Using the MGF of Exponential Distribution]

$$= G_{\Phi'} \left[\frac{1}{1 + \frac{\gamma d_i^{-\alpha}}{d_1^{-\alpha}}} \right]$$

Combining the above 2 results, we get the expression of the Coverage Probability, thereby completing this proof. $\qquad \square$

4.3   Applications for BLCP Network

We can directly apply the framework and the results demonstrated in Theorem 4, to our BLCP model to generate the results. The only prerequisite is we must derive an expression for the PGFL of the interference terms used in the same theorem.

So, we need to evaluate: $G_{\Phi'} \left[\frac{1}{1 + \frac{\gamma d_i^{-\alpha}}{d_1^{-\alpha}}} \right]$ for our BLCP Process.

We begin by noting that, from Equation 3.5 for a general monotonic function f(x):

$$PGFL_\Phi = G(x_t, R, n_B)$$

$$= \left[\frac{\int_0^{2\pi} \int_0^R exp\left(-2\lambda \int_0^\infty 1 - f\left(\sqrt{y^2 + (x_t cos\theta - r)^2}\right) dy\right) dr \, d\theta}{2\pi R} \right]^{n_B}$$

In this expression, the integrations over the (r, θ) pair, is to average out the results over the n_B randomly generated BLP lines.

The actual PLCP points are being considered by inner integral over 'y', which represents the distance of the point from the midpoint of the chord (Please refer to Fig 3.2 for reference).

Referring back to the proof for Equation 3.5, $|x_t \cos \theta - r|$ was the distance of the BLP line from $(x_t, 0)$ and y was the distance of the point along the line. Thus total distance of the BLCP point from $(x_t, 0)$ is:

$$d = \sqrt{y^2 + (x_t cos\theta - r)^2} \tag{4.3}$$

Putting, d = d_1 in Equation 4.3, we get:

$$y = \sqrt{d_1^2 - (x_t cos\theta - r)^2} \tag{4.4}$$

If start counting the PLCP points from y, as given in Equation 4.4 we would essentially ensure the only PLCP points with a total distance $> d_1$ are counted. So, for $PGFL_{\Phi'}$, we get:

$$G_{\Phi'} = \left[\frac{\int_0^{2\pi} \int_0^R exp\left(-2\lambda \int_{\sqrt{d_1^2-(x_t cos\theta-r)^2}}^\infty 1 - f\left(\sqrt{y^2 + (x_t cos\theta - r)^2}\right) dy\right) dr \, d\theta}{2\pi R} \right]^{n_B} \tag{4.5}$$

As we notice from Equation 4.5, that this expression is a function of the random variable 'd_1', so we have to take an expectation over d_1 as well.

Combining all of these and simplifying we get:

$$P_{Coverage} = \mathop{\mathbb{E}}_{d_1} \left[\exp \left(\frac{-\gamma N_0}{K P d_1^{-\alpha}} \right) G_{\Phi'} \left(\frac{1}{1 + \frac{\gamma d_i^{-\alpha}}{d_1^{-\alpha}}} \right) \right]$$

$$= \mathop{\mathbb{E}}_{d_1} \left[\exp \left(\frac{-\gamma N_0}{K P d_1^{-\alpha}} \right) G_{\Phi'} \left(\frac{d_1^{-\alpha}}{d_1^{-\alpha} + \gamma d_i^{-\alpha}} \right) \right]$$

Where: $G_{\Phi'} \left(\dfrac{d_1^{-\alpha}}{d_1^{-\alpha} + \gamma d_i^{-\alpha}} \right)$

$$= \left[\frac{\int_0^{2\pi} \int_0^R exp \left(-2\lambda \int_{\sqrt{d_1^2 - (x_t cos\theta - r)^2}}^{\infty} \left(1 - \frac{d_1^{-\alpha}}{d_1^{-\alpha} + \gamma \left[y^2 + (x_t cos\theta - r)^2 \right]^{-\frac{\alpha}{2}}} \right) dy \right) dr\, d\theta}{2\pi R} \right]^{n_B}$$

$$= \left[\frac{\int_0^{2\pi} \int_0^R exp \left(-2\lambda \int_{\sqrt{d_1^2 - (x_t cos\theta - r)^2}}^{\infty} \left(\frac{\gamma \left[y^2 + (x_t cos\theta - r)^2 \right]^{-\frac{\alpha}{2}}}{d_1^{-\alpha} + \gamma \left[y^2 + (x_t cos\theta - r)^2 \right]^{-\frac{\alpha}{2}}} \right) dy \right) dr\, d\theta}{2\pi R} \right]^{n_B}$$

(4.6)

Before going on, we would like to reiterate that, this expression for $G_{\Phi'}$ is terms of d_1, or rather more accurately we have calculated: $\mathbb{E}_{\Phi'} \left(\prod_{\Phi'} \left(f(\text{SINR} \mid \text{min. dist.} = d_1) \right) \right)$. So, we have used a bit of abuse of notation to represent this simply as $G_{\Phi'}$.

The only problem with this expression is it is too complicated to solve analytically, so we numerically evaluated the results which are presented in the next section.

4.4 Simulation Results

We begin with a comparative analysis of BLCP v/s PLCP Models under 2 different values of α (2.5 and 4) to highlight the differences (Please refer to Figure 4.1) between the 2 models. The Noise intensity is kept at -204 dB to make the environment predominantly interference dominant.

Immediately there are a few key points which are apparent from this simulation:

- PLCP results are uniform irrespective of the location of the typical user. However, for BLCP, the location of the typical user with respect to the city absolutely matters.
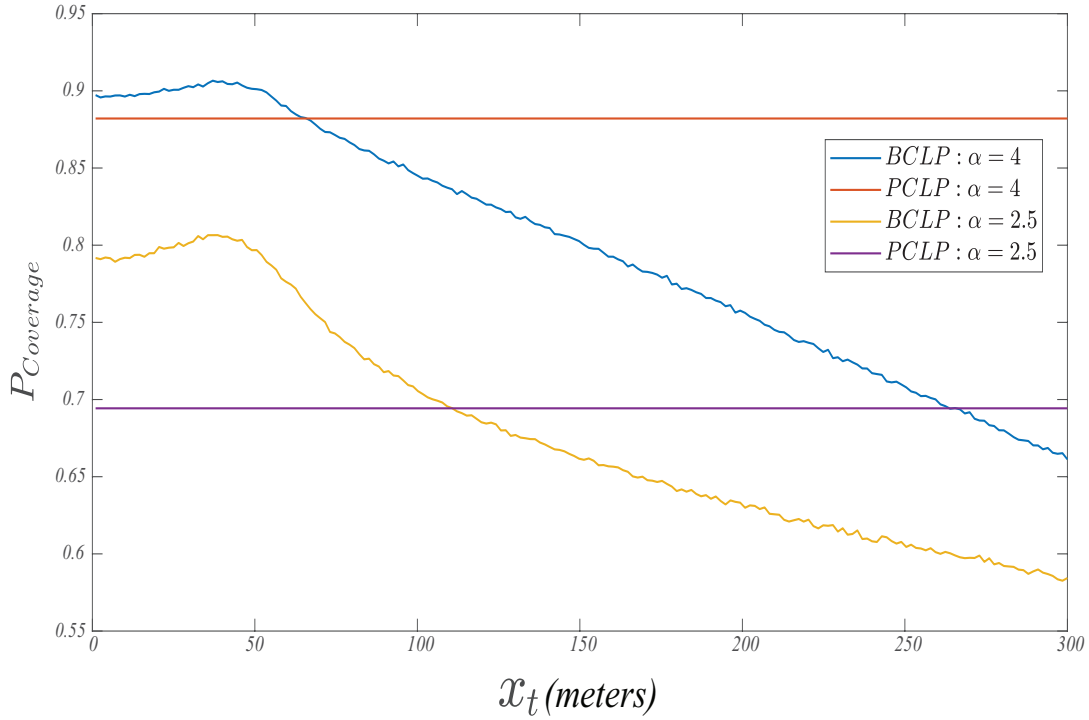
Fig. 4.1. Simulated BLCP and PLCP Networks with $n_B = 10$, R = 50, $\alpha = 2.5$ and $4, \lambda = 0.01$, P = -10 dB, K = 10^{-5} and $N_0 = -204$ dBW/Hz

- Towards the city center, where there is a relatively higher density of streets and thus, access points, we have more interference. Towards the periphery of the city, the mean distance from the nearest access points increase, thus reducing received power overall. Thus, SINR Coverage is a fine balance between less interference v/s more received power. However, this does not matter at all for a PLCP Process, due to its uniformity.

- Since for BLCP, we have more access points towards the center of the region, the mean distance is lower. Hence, BLCP consistently gives higher SINR coverage Probability than PLCP model, till we move out far enough that average distance from access points increase enough to make the PLCP model give better coverage.

4.4.1 Effect of Path Loss Coefficient (α)

Higher α value, means less received power for similar distance, and thus it penalizes access points which are further away. In context of this simulation, inside the city, higher α value means less interference and thus higher SINR Coverage. This holds true for both BLCP and PLCP model. As we move further out from the city, we see that the difference in coverage probability between the 2 plots keep reducing as the average distance is more. However, this being a predominantly interference driven network, lower α values strictly means more interference and thus lower SINR, even moderately far from the city center.
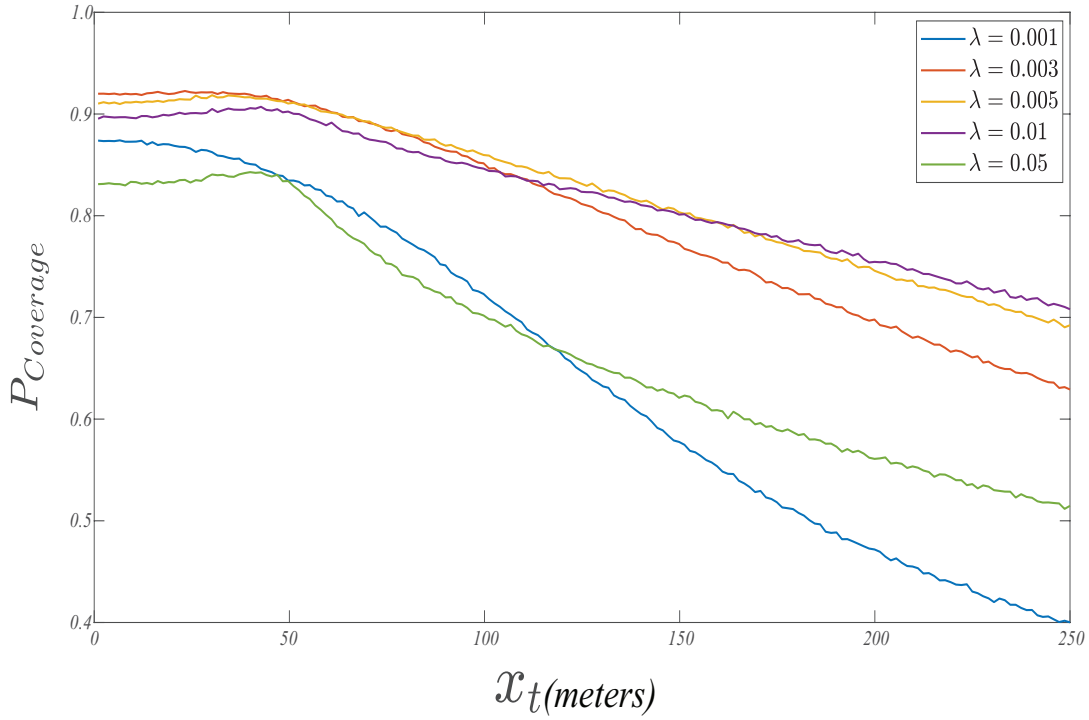
Fig. 4.2. Simulated BLCP network with n_B = 10, R = 50, α = 4, $\lambda = 0.001$, $0.003, 0.005, 0.01$ and 0.05, P = -10 dB, K = 10^{-5} and $N_0 = -204$ dBW/Hz

4.4.2 Effect of Network Density along roads (λ)

Next, we study the effect of access point density across the street or λ over the overall SINR coverage.

Increasing the density of access points along a line, decreases the mean distance to the the nearest access point for a typical user. This in turn increases received signal strength. However, more power for the nearest access point generally means more power for the interferers as well. So, too many access points can create poor coverage due to low SINR. But, if we have too few access points, even that results in a poor coverage, due to greater average distance to nearest access point.

This point is perfectly demonstrated by Figure 4.2 :

- $\lambda = 0.05$: Too high intensity, poor SINR Coverage due to interference.

- $\lambda = 0.001$: Too low intensity, poor SINR Coverage due to nearest access point being far away.

- $\lambda = 0.01$: This intensity was performing best for the regions outside the central area, where interference is minimal, due to a lower density of streets. However, inside the central region, due to high interference, we don't have equally good coverage, as compared to the periphery.

- $\lambda = 0.003 - 0.005$: 0.003 is just about low enough for the dense central region, to give the best performance there, though both $\lambda = 0.01$ and $\lambda = 0.03$ are

performing better than $\lambda = 0.01$ for the same region. However, when we move on to the periphery of the city towards its suburbs, where interference is not that big of an issue, the performance drops due to lower density.

So, one way to optimize this coverage can be to have unequal network access point densities inside and outside the cities, to counteract the effect of dense road networks. In our example, $\lambda = 0.003$ (3 access points/Km of a road) inside the city and $\lambda = 0.01$ (1 access point every 100 m of the road) for the less densely packed suburbs of the city, is the most optimal way to give coverage to users in the entire region.

With all these simulations, there is one more point to note: The coverage slightly increases as we go from within the city center towards the periphery, peaking at the edge of the city, and then dropping sharply as we move out into the suburbs. This can be explained again as a consequence of interference. The more we move towards the city center, the more densely packed the roads are, which leads to more interference. But, as we move outside, the road density, and thus overall SINR falls due to lower received power.

4.4.3 Effect of Noisy Channel

All the simulations and discussions we had so far, assumed an interference dominated channel. In this section, we explore what happens in case of a noisy channel with significant noise.
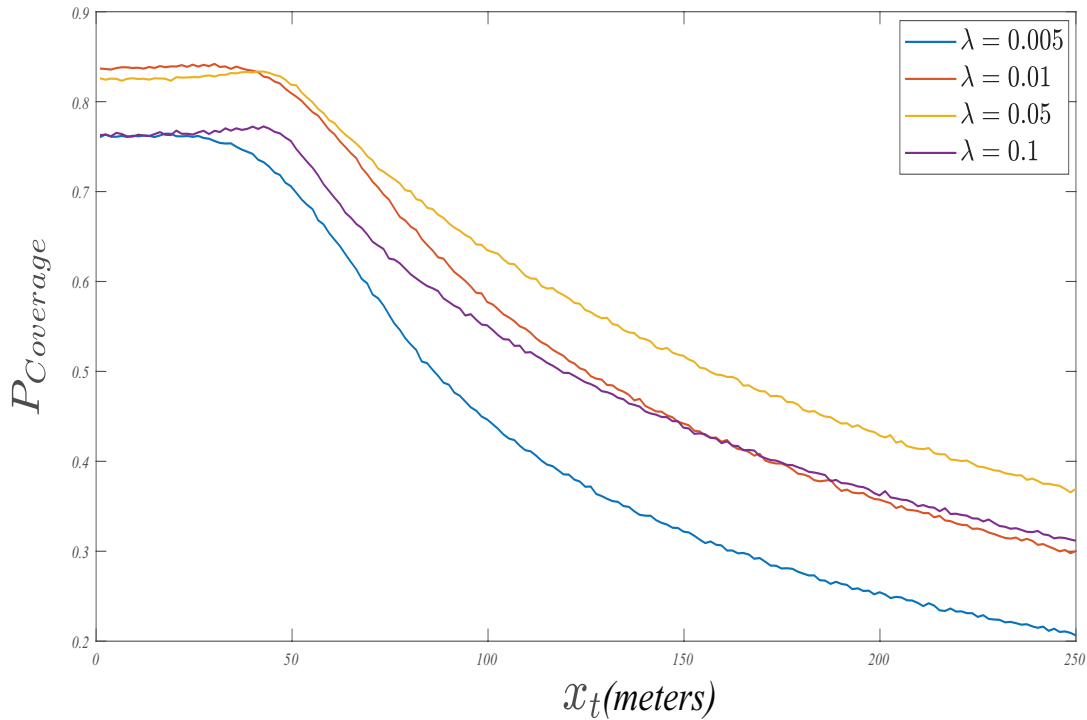

Fig. 4.3. Simulated BLCP network with $n_B = 10$, R = 50, $\alpha = 4$, $\lambda = 0.005$, $0.01, 0.05$ and 0.1, P = -10 dB, K = 10^{-5} and $N_0 = -184$ dBW/Hz

28

We have simulated the network with -184 dBW/Hz of noise this time, as opposed to -204 dBW/Hz, that we used previously. When there is more noise, the effect of interference on the overall SINR reduces. So, with a noisy channel, proximity to a base station is more important, compared to interference.

So, as we can see from the Figure 4.3, $\lambda = 0.01$ is performing the best in the central region, but the coverage drops sharply outside the dense city area due to increasing distance and high noise. Lower values of λ (like $\lambda = 0.005$), gives too much noise, but with high values, like $\lambda = 0.1$, we again face issues due to interference. The best results are obtained with $\lambda = 0.01$ for dense central region and $\lambda = 0.05$, for the periphery.

Thus, overall the pattern is the same: Less Dense urban access point setup with more dense access points for suburban region. The only added difference is:

The base line values of base station intensity needed to achieve comparable coverage to the previous case, is more here to compensate for the higher noise overall. This result is as we should intuitively expect.

Chapter 5

Conclusion and Future Scope

We started out to address the challenges faced by current stochastic geometry based network models to model heterogeneous networks like modern urban cities. Specifically, we started with the inadequacies of PLCP process which motivated us to look into and develop metric for a new line process to model heterogeneous networks, called the BLCP, which we have introduced here.

Throughout the work, we have derived multiple results pertaining to the line process we introduced, leading upto the PGFL analysis for the model. Leveraging which, we were able to conduct a SINR coverage analysis of the model, to see how it compares to the existing models like PLCP. This allowed us to gain some valuable insight on network densities related to optimum coverage throughout under different channel conditions.

The model outlined in this thesis, provides first basic framework for network analysis for heterogeneous network densities resembling modern urban population trends. Going forward, this model can be integrated with other models like the lily-pond model, Poisson stick process etc., to develop an even more accurate framework for network modelling.

Also, this work has assumed a general network model, without any underlying nuances like UAV Networks, Vehicular networks, blockages etc. There exists a rich literature on these specific types of network. We plan to apply our model to these specific networks, to see how heterogeneous networks impact these types of networks.

Bibliography

[1] T. Maksymyuk *et al.*, "Stochastic geometry models for 5G heterogeneous mobile networks," *SmartCR*, vol. 5, pp. 89–101, 2015.

[2] M. J. Farooq *et al.*, "A stochastic geometry model for multi-hop highway vehicular communication," *IEEE Transactions on Wireless Communications*, vol. 15, no. 3, pp. 2276–2291, 2015.

[3] J. G. Andrews *et al.*, "A primer on cellular network analysis using stochastic geometry," *arXiv preprint arXiv:1604.03183*, 2016.

[4] M. Di Renzo, "Stochastic geometry modeling and analysis of multi-tier millimeter wave cellular networks," *IEEE Transactions on Wireless Communications*, vol. 14, no. 9, pp. 5038–5057, 2015.

[5] F. Baccelli *et al.*, "Stochastic geometry and architecture of communication networks," *Telecommunication Systems*, vol. 7, no. 1, pp. 209–227, 1997.

[6] F. Morlot, "A population model based on a Poisson line tessellation," in *IEEE WiOpt*, May 2012, pp. 337–342.

[7] V. V. Chetlur Ravi, "Stochastic geometry for vehicular networks," Ph.D. dissertation, Virginia Tech, 2020.

[8] J. P. Jeyaraj and M. Haenggi, "Cox models for vehicular networks: Sir performance and equivalence," *IEEE Transactions on Wireless Communications*, vol. 20, no. 1, pp. 171–185, 2020.

[9] C. Gloaguen *et al.*, "Analysis of shortest paths and subscriber line lengths in telecommunication access networks," *Networks and Spatial Economics*, vol. 10, no. 1, pp. 15–47, 2010.

[10] C.-S. Choi and F. Baccelli, "An Analytical Framework for Coverage in Cellular Networks Leveraging Vehicles," *IEEE Trans. Commun.*, vol. 66, no. 10, pp. 4950–4964, Oct. 2018.

[11] G. Ghatak *et al.*, "Modeling and analysis of hetnets with mm-wave multi-rat small cells deployed along roads," in *GLOBECOM 2017-2017 IEEE Global Communications Conference.* IEEE, 2017, pp. 1–7.

[12] G. Ghatak, A. De Domenico, and M. Coupechoux, "Small cell deployment along roads: Coverage analysis and slice-aware rat selection," *IEEE Transactions on Communications*, vol. 67, no. 8, pp. 5875–5891, 2019.

[13] H. S. Dhillon and V. V. Chetlur, *Poisson Line Cox Process: Foundations and Applications to Vehicular Networks*.   Morgan & Claypool Publishers, 2020.